International Journal of Solids and Structures 47 (2010) 2872–2883

Contents lists available at ScienceDirect

International Journal of Solids and Structures

journal homepage: www.elsevier.com/locate/ijsolstr

On the compressive strength of open-cell metal foams with Kelvin and random cell structures

Wen-Yea Jang [a], Stelios Kyriakides [a,*], Andrew M. Kraynik [b]

[a] Research Center for Mechanics of Solids, Structures and Materials, The University of Texas at Austin, United States
[b] Sandia National Laboratories, Albuquerque, NM 87185, United States

ARTICLE INFO

Article history:
Received 20 January 2010
Received in revised form 15 June 2010
Available online 23 June 2010

Keywords:
Foams
Aluminum
Elastic properties
Strength

ABSTRACT

Two families of finite element models of anisotropic, aluminum alloy, open-cell foams are developed and their predictions of elastic properties and compressive strength are evaluated by direct comparison to experimental results. In the first family of models, the foams are idealized as anisotropic Kelvin cells loaded in the <100> direction and in the second family more realistic models, based on Surface Evolver simulations of random soap froth with N^3 cells are constructed. In both cases the ligaments are straight but have nonuniform cross sectional area distributions that resemble those of the foams tested. The ligaments are modeled as shear deformable beams with elasto-plastic material behavior. The calculated compressive response starts with a linearly elastic regime. At higher stress levels, inelastic action causes a gradual reduction of the stiffness that eventually leads to a stress maximum, which represents the strength of the material. The periodicity of the Kelvin cell enables calculation of the compressive response up to the limit stress with just a single fully periodic characteristic cell. Beyond the limit stress, deformation localizes along the principal diagonals of the microstructure. Consequently beyond the limit stress the response is evaluated using finite size 3-D domains that allow the localization to develop. The random models consist of 3-D domains of 216, 512 or 1000 cells with periodicity conditions on the compressed ends but free on the sides. The compressive response is also characterized by a limit load instability but now the localization is disorganized resembling that observed in experiments. The foam elastic moduli and strengths obtained from both families of models are generally in very good agreement with the corresponding measurements. The random foam models yield 5–10% stiffer elastic moduli and slightly higher strengths than the Kelvin cell models. Necessary requirements for this high performance of the models are accurate representation of the material distribution in the ligaments and correct modeling of the nonlinear stress–strain response of the aluminum base material.

1. Introduction

Open-cell foams have a complex microstructure consisting of an interconnected network of ligaments that form along the edges of randomly packed cells that evolve during the foaming process. As reported in Matzke's pioneering work on soap froth [1946], the cells are irregular polyhedra with anywhere from 11 to 17 faces when the foam is nearly monodisperse. In the case of solid foams, the material is concentrated in the nearly straight edges of the polyhedra and in the nodes where they intersect, usually four at a time. This microstructure gives such foams unique mechanical, thermal, acoustical and other properties (e.g., see Hilyard and Cunningham, 1994; Gibson and Ashby, 1997; Weaire and Hutzler, 1999; Ashby et al., 2000). Connecting the microstructure to these properties is an enabling step in the design of solid foams. These objectives have been pursued by detailed studies of a class of polymeric open-cell foams (Gong et al., 2005a; Gong and Kyriakides, 2005, 2006) and more recently of metallic foams (Jang and Kyriakides, 2009I,II–referred to as J & K-09I and J & K-09II henceforth). Here we will present additional results for metallic foams.

The foams under study are Aluminum (Al-6101-T6) Duocel® open-cell foams manufactured by ERG with relative densities of about 8%. A typical image of the microstructure of such foams generated with computed X-ray tomography is shown in Fig. 1. This type of foam is thought to be made using polymeric foams as templates to generate a mold in which aluminum alloy is cast (see Section 2.5 Ashby et al., 2000). Consequently it retains characteristics such as cell size uniformity, type of polyhedra, ligament length distribution, etc., exhibited by commercially available polymeric

* Corresponding author. Address: Research Center for Mechanics of Solids, Structures and Materials, WRW 110, C0600, The University of Texas at Austin, Austin, TX 78712, United States.
E-mail address: skk@mail.utexas.edu (S. Kyriakides).

0020-7683/$ - see front matter © 2010 Elsevier Ltd. All rights reserved.
doi:10.1016/j.ijsolstr.2010.06.014

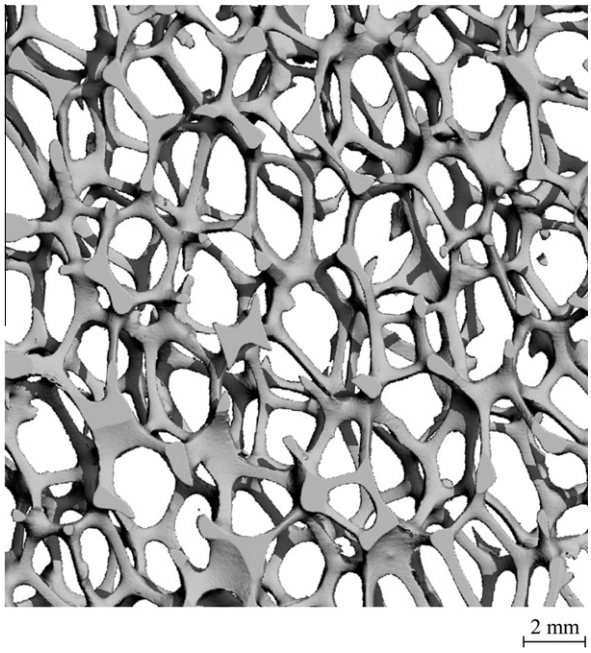

Fig. 1. Computed tomography image of a 10-ppi Al foam (ρ^*/ρ = 8.23%).

foams (see comparison of geometric characteristics of polymeric and Al foams in Jang et al. (2008)). The typical compressive stress-(σ_{11} = force/undeformed area) displacement (δ_1/H_1) response of such a foam is shown in Fig. 2. It consists of a nearly linear elastic regime that terminates into a limit load (σ_l). This is followed by a load plateau that extends to an average strain of about 50–55%, followed by a second stiff branch (*densification*). The low initial stress peak and extended load plateau are responsible for the superb energy absorption characteristics of such foams.

In our most recent work (J & K-09I and J & K-09II) the foam microstructure was idealized using the 14-sided regular cell of Kelvin (Thompson, 1887). It was demonstrated that most aspects of compressive response, such as the one in Fig. 2, can be reproduced using suitable domains of this model foam. This was achieved by assigning ligament and cell geometric properties representative of those of the actual foam studied, along with the elasto-plastic properties of the Al alloy base material, to the Kelvin cell foam. The present results are a continuation of this work in which random soap froth microstructures generated using the Surface Evolver software (Brakke, 1992) are similarly modeled. The random

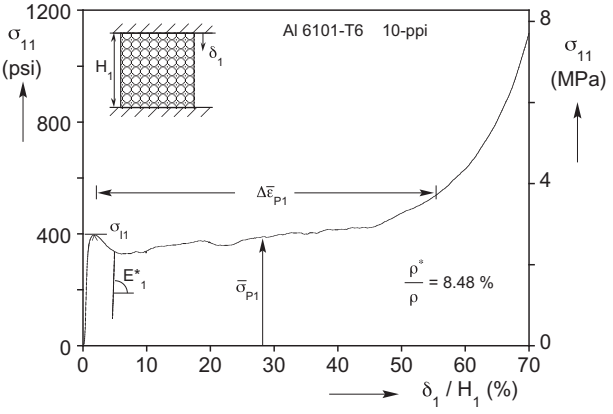

Fig. 2. Typical compressive response of an Al alloy open-cell foam (crushing in the rise direction).

foam models are used to establish the elastic properties and the "strength" of such foams. The results are evaluated by direct comparison to measured properties and are also critically compared to corresponding results from the Kelvin cell models.

2. Background

2.1. Review of the morphology of aluminum foams

Computed X-ray tomography was used to characterize the foam microstructure including cell size, distribution, anisotropy, ligament length and cross sectional area distributions as described in Jang et al. (2008). Here we will summarize the findings that are required in the modeling effort that follows. Three foams of the same alloy and heat treatment with nominal cell sizes of 10-, 20- and 40-ppi and respective average relative densities (ρ^*/ρ) of 8.23%, 7.50% and 7.54% were analyzed. As can be seen in the foam image in Fig. 1, the polyhedral cells are elongated in the rise direction of the polymeric foam template. Average anisotropy values $\lambda = h_1/h_2$ of 1.27, 1.24 and 1.18 are reported in Table 1 (h_1 and h_2 defined in cell image below Table 1 and $\bar{h}_1$ is the average height of the cells). Given in the table is also a measure of *polydispersity* based on the ratio of one standard deviation of the average cell height (Σ_{h_1}) normalized by $\bar{h}_1$. The results range from 0.0707 to 0.0754 indicating that cell size variation is small in these foams (i.e., nearly monodisperse). Furthermore, from comparisons of the microstructures of the three foams it was concluded that at least to first order they scale with cell size (Fig. 5 in J & K-09I).

The irregular polyhedral nature of the cells is illustrated in Fig. 1. As reported earlier the ligaments of these foams have rounder convex boundaries (see Fig. 11 in Jang et al. (2008)). The areas of many ligament cross sections $A(\xi)$ were measured digitally as a function of the axial position $\xi = x/\ell$ and the results were fitted with the following symmetric expression (Fig. 14 of Jang et al. (2008)):

$$A(\xi) = A_o f(\xi) = A_o\left(36\xi^4 + \xi^2 + 1\right) \tag{1}$$

A_o in turn was found to vary with ligament length in the manner shown in Fig. 15 of Jang et al. (2008). (The normalizing values $\overline{A}_o$ and $\bar{\ell}$ for each foam and their standard deviations are listed in Table 1.) The measurements were fitted as follows:

$$A_o(\eta) = \overline{A}_o g(\eta) = \overline{A}_o\left(0.6633 + 0.2648\eta^{-2.5963}\right), \quad \eta = \ell/\bar{\ell} \tag{2}$$

2.2. Compression experiments

2.0 × 2.0 × 2.0 in (51 × 51 × 51 mm) specimens were extracted from large blocks of foam using a computer operated wire EDM system. The process minimizes distortion along the cut edges and improves the parallelity of the two loaded surfaces. In order to minimize the influence of the edges on the initial response, Al alloy plates were bonded to the two surfaces that were subsequently loaded. The specimens were compressed between parallel platens in a stiff electromechanical testing machine run under displacement control. The typical displacement rate was $\dot{\delta}/H = 8.3 \times 10^{-4}\ s^{-1}$ (corresponds to the strain rate when the deformation is homogeneous; H = height of the specimen). Because the foam density varied slightly within the mother foam blocks the relative densities of individual specimens will be reported (see Tables 2 and 3).

Fig. 3 shows the early parts ($\delta/H \leqslant 0.12$) of a pair of representative stress–displacement responses obtained from rise and transverse direction compression tests on 10-ppi foam specimens. The rise direction response is seen to exhibit an initial nearly linear part during which the deformation is essentially homogeneous. At approximately a stress of 300 psi (2.07 MPa) bending and

Table 1
Geometric parameters of Al-6101-T6 foams analyzed.

Foam ppi	ρ^*/ρ (%)	$\bar{h}_1$ in (mm)	$h_1\|_{\min-\max}$ in (mm)	$\Sigma_{h_1}/\bar{h}_1$	λ	$\bar{\ell}$ in (mm)	$\Sigma_\ell/\bar{\ell}$	$\overline{A}_o \times 10^3$ in^2 (mm^2)	$\Sigma_{A_o}/\overline{A}_o$
10	8.23	0.184 (4.683)	0.158–0.234 (4.013–5.944)	0.0754	1.27	0.070 (1.780)	0.263	0.459 (0.296)	0.261
20	7.50	0.141 (3.570)	0.120–0.170 (3.048–4.318)	0.0707	1.24	0.048 (1.22)	0.277	0.144 (0.0929)	0.235
40	7.54	0.115 (2.929)	0.087–0.136 (2.210–3.454)	0.0749	1.18	0.041 (1.04)	0.268	0.0648 (0.0418)	0.238

$\rho = 0.0972$ lb/in^3 (2690 kg/m^3).

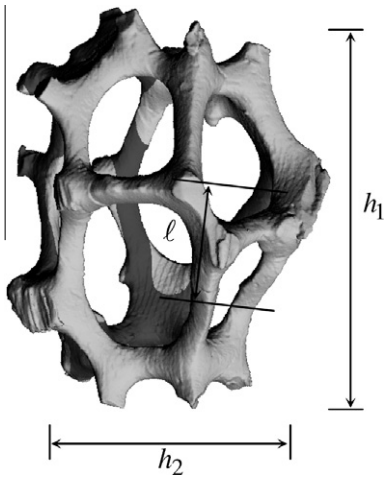

stretching cause plastification in some of the ligaments and the material stiffness becomes progressively smaller. Indeed a stress maximum develops at a stress of 396 psi (2.73 MPa) after which the stress drops to a local minimum and then follows a relatively flat stress plateau until the crushing has consumed the whole specimen or the material has densified (see Fig. 2). The stress maximum, henceforth called *initiation stress* (σ_{I1}) or the foam *strength*, represents the onset of localized deformation associated with buckling of ligaments in localized bands. This is demonstrated in Fig. 4 that shows the undeformed (⓪) and two deformed images obtained using X-ray tomography. The images show a slice of the material approximately 6 mm thick in a neighborhood that develops an inclined band of initially buckled ligaments that later lead to the collapse of the affected cells. Image ① was taken at $\delta/H = 10\%$ in order for the ligament buckling and cell crushing in

Table 2
Measured mechanical properties of Al-6101-T6 foams in the rise direction.

Exp. No.	ρ^*/ρ (%)	E_1^*/E(%)	σ_{I1} psi (MPa)
(a)			
10 ppi, $\lambda = 1.27$			
R10–1	8.33	0.865	396 (2.73)
R10–2	8.79	0.857	456 (3.14)
R10–3	8.63	0.863	446 (3.08)
R10–4	8.48	0.871	396 (2.73)
(b)			
20 ppi, $\lambda = 1.24$			
R20–1	8.26	0.705	352 (2.43)
R20–2	7.47	0.677	283 (1.95)
R20–3	8.43	0.779	379 (2.61)
R20–4	8.37	0.857	369 (2.54)
(c)			
40 ppi, $\lambda = 1.18$			
R40–1	7.98	0.660	339 (2.34)
R40–2	8.20	0.746	360 (2.48)
R40–3	8.24	0.780	393 (2.71)
R40–4	8.18	0.733	406 (2.80)

$E = 10^4$ ksi (69 GPa), $\nu = 0.3$.

Table 3
Measured mechanical properties of Al-6101-T6 foams in the transverse direction.

Exp. No.	ρ^*/ρ (%)	E_2^*/E (%)	σ_{I2} psi (MPa)
(a)			
10 ppi, $\lambda = 1.27$			
T10–1	8.56	0.466	290 (2.00)
T10–2	8.48	0.493	298 (2.05)
T10–3	8.74	0.527	333 (2.30)
(b)			
20 ppi, $\lambda = 1.24$			
T20–1	7.36	0.459	297 (2.05)
T20–2	7.67	0.426	308 (2.12)
T20–3	7.70	0.479	309 (2.13)
(c)			
40 ppi, $\lambda = 1.18$			
T40–1	8.22	0.570	294 (2.03)
T40–2	8.03	0.506	323 (2.23)
T40–3	8.03	0.538	289 (1.99)

$E = 10^4$ ksi (69 GPa), $\nu = 0.3$.

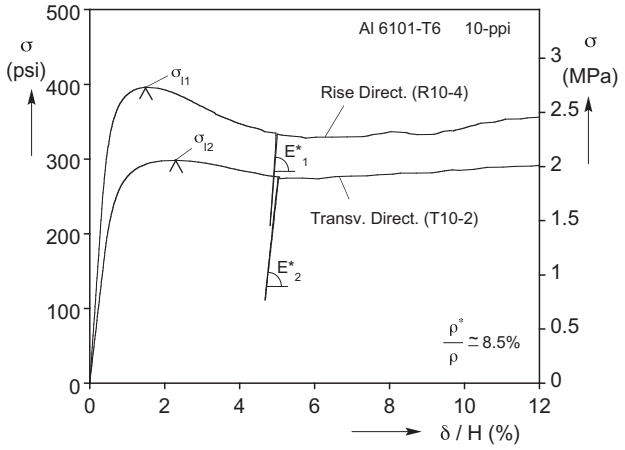

Fig. 3. Comparison of compressive responses in the rise and transverse directions.

the middle to be visible. The band is inclined but has a fully three-dimensional relief that is dictated by small imperfections in the microstructure. In image ②, taken at $\delta/H = 17\%$, the banded crushing is now fully developed affecting several cells. During the subsequent stress plateau the buckling and crushing gradually spread to previously intact material (see J & K-09I for evolution of crushing). At an average strain of 5% the specimen was unloaded and the unloading response was used to measure the elastic modulus of the material, E_1^*, as this was found to yield more accurate and reproducible values of this variable than the initial elastic loading part of the response. The variables E_1^*, σ_{I1} are listed in Table 2 under specimen R10–4 (see also Zhou et al., 2002; Zhou et al., 2004).

The response in the transverse direction is similar except the elastic modulus, E_2^*, is smaller (0.00493E vs. 0.00871E where E is the modulus of the Al alloy—10^4 ksi—69 GPa) and the rest of the response traces lower stress levels. Thus, the initiation stress, σ_{I2}, is now only 298 psi (2.05 MPa). However, as reported in J & K-09I the events associated with this response are similar to those observed for the rise direction. In other words, beyond the stress maximum the deformation localizes in disorganized bands that broaden gradually covering the whole specimen as the stress plateau evolves.

A total of twelve crushing tests, four for each foam, were performed in the rise direction and the results are summarized in Table 2. As mentioned above, the density varied somewhat within each foam block and this affected the measurements to the degree shown in the Table. Fig. 5(a) shows responses from specimens with different cell size chosen to have approximately the same density. In these cases the responses are very similar supporting the premise that properties do not depend on cell size. The measured strengths (σ_{I1}) are plotted against relative density in Fig. 6(a) where, because of the narrow range of ρ^* considered, they are seen to follow nearly linear trajectories.

Nine compression experiments were also conducted in the transverse direction and the results are summarized in Table 3. Fig. 5(b) shows a comparison of three responses from foams of different cell size with a relative density of approximately 8.0%. They are seen to be very similar supporting the previously made statements. The strengths (σ_{I2}) are plotted against density in Fig. 6(b) where once again they are seen to have a nearly linear trend (similar plots of the elastic moduli E_1^* and E_2^* appear in Figs. 14(a) and 21(a) of J & K-09I respectively).

3. Modeling of the foams

The Al foams studied will be modeled first by adopting the perfectly ordered structure, based on Kelvin's 14-sided cell shown in

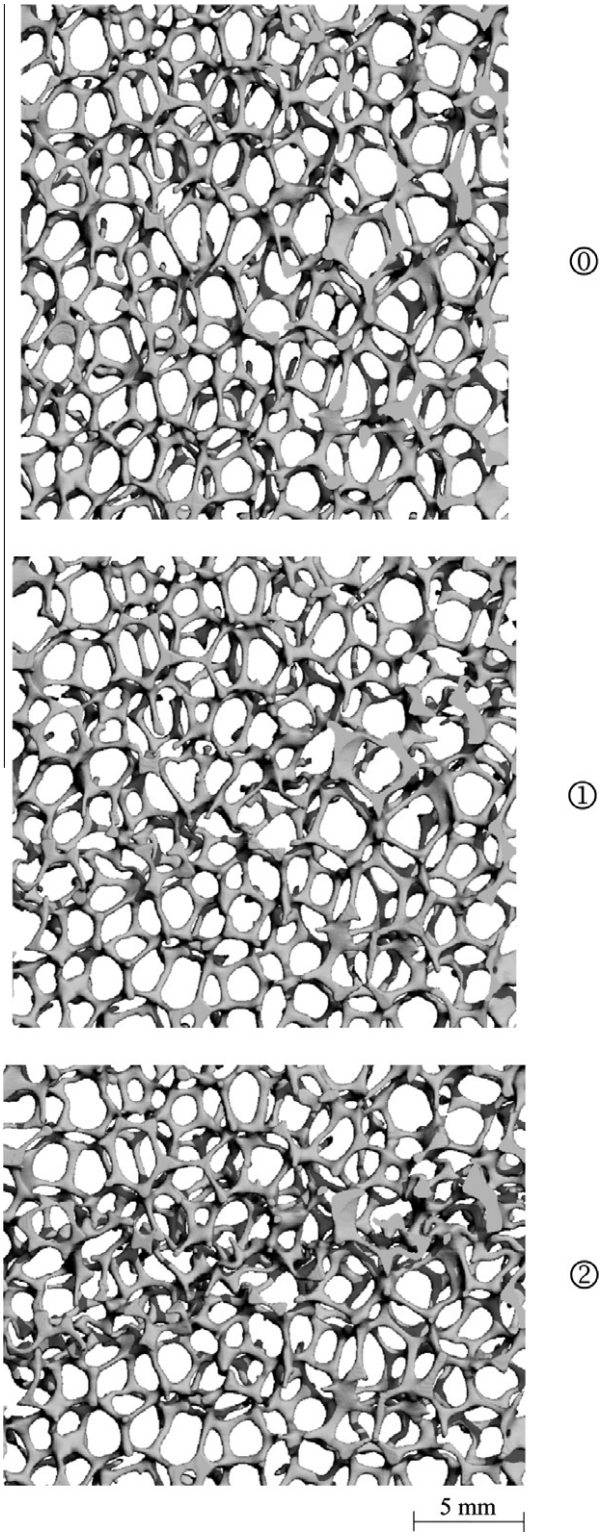

Fig. 4. The initial and two deformed configurations corresponding to the rise direction compressive response R10–4 shown in Fig. 3. Note the bending and buckling of ligaments in configurations ① and ②.

Fig. 7 loaded in the <100> and <010> directions, henceforth referred to as "Kelvin" (also used in J & K-09II and previously by Gong and Kyriakides (2005) and Gong et al. (2005b) in the modeling of polymeric foams).

The second model used consists of clusters of Kelvin cells with randomly perturbed vertices; it will be referred to as "perturbed Kelvin." Here the coordinates of all the nodes of a finite size do-

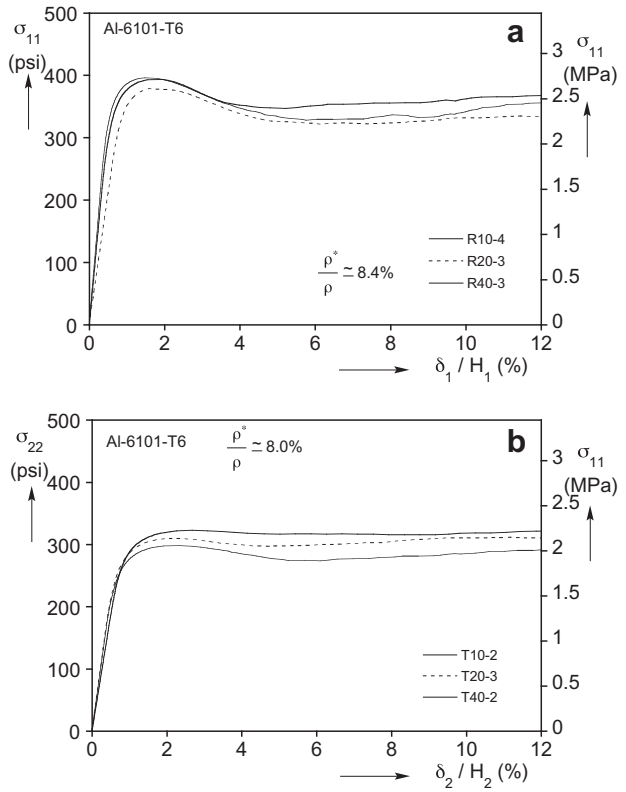

Fig. 5. (a) Comparison of rise direction compressive responses from specimens of different cell sizes. (b) Comparison of transverse direction compressive responses from specimens of different cell sizes.

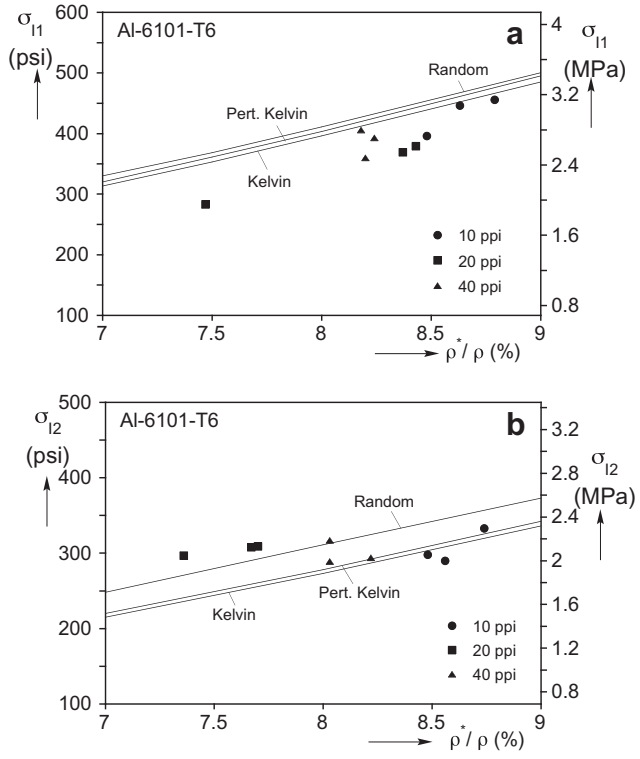

Fig. 6. Al foam measured and calculated initiation stresses as a function of relative density: (a) σ_{I1} and (b) σ_{I2}.

main of Kelvin cells are perturbed as follows. The position vector in the perturbed configuration, $\boldsymbol{x}$, is given by:

$$\boldsymbol{x} = \boldsymbol{x}_o + p\xi\ell, \quad 0 \leqslant \xi_i \leqslant 0.5, \quad i = 1,3 \tag{3}$$

where $\boldsymbol{x}_o$ is the initial position vector of a node, $\boldsymbol{x}$ is the perturbation and p is a normally distributed random number between -0.5 and 0.5 (in the results that follow $\xi_i = \xi_o$, $i = 1,3$). The disturbance applied to the nodes on opposite faces of the domain is chosen so as to accommodate periodic boundary conditions (see Jang et al., 2008 for more details).

The most realistic models analyzed are based on the microstructure of random spatially periodic soap froth simulated with Brakke's *Surface Evolver* (1992) (Kraynik et al., 2003), and is referred to as "random." As reported in Jang et al. (2008), the process generates a foam skeleton that is very representative of actual foam microstructures as demonstrated in the cluster of cells shown in Fig. 8(a). In other words, the types of polyhedra present in the model, the distribution of different polygonal cell faces, and the distribution of ligament lengths compare very well with measurements made in polymeric foams. (Appendix A presents an outline of the numerical steps involved in generating such random foams). Details of the main geometric characteristics of the models follow.

3.1. Ligament geometry

The ligaments in all models will be assumed to have circular cross sections (radius R) with the area distribution given in (1) (see J & K-09II for justification).

3.2. Anisotropy

Anisotropy is introduced to the three model foams as follows. All ligaments with a projection in the x_1-direction are elongated so that this projection is amplified by the factor λ while the projections in the x_2- and x_3- directions remain the same. Thus, for example, the Kelvin cell height becomes $h_1 = 2\sqrt{2}\ell\tan\alpha$ while the width remains $h_2 = 2\sqrt{2}\ell$, where

$$\frac{h_1}{h_2} = \tan\alpha = \lambda \tag{4}$$

as shown in Fig. 7 (see also Dement'ev and Tarakanov, 1970b; Gong and Kyriakides, 2005). Fig. 8(b) shows how an anisotropy of $\lambda = 1.3$ alters the cluster of random cells shown in Fig. 8(a).

3.3. Correction for the volume of material in the nodes

When ligaments are modeled as beams that connect four to each node, the ends of the beams overlap. Jang et al. (2008) removed the overlap material by cutting the ends of the beams (see Refs. for details). With this correction, the relative density relates to the ratio of the radius at mid-span of ligaments, R_o, and the length, ℓ, through

$$\frac{\rho^*}{\rho} = k\left(\frac{R_o}{\ell}\right)^n \tag{5}$$

where n depends on the anisotropy ($n \neq 2$). Table 4 lists k and n for anisotropy values $1 \leqslant \lambda \leqslant 1.3$.

For a foam of a required density and anisotropy R_o is evaluated from Eq. (5) using the ligament length of the initial isotropic Kelvin cell. A_o depends on ℓ, which is introduced in the following approximate manner. The average length of all ligaments ($\bar{\ell}$) in any model is first calculated. The lengths are then grouped into those longer and those shorter than $\bar{\ell}$, and the average length of each category ($\bar{\ell}_1, \bar{\ell}_2$) is established. The two average lengths are then used in Eq. (2) to establish corresponding values for A_o. The effect of this change on the foam density, if any, is not considered.

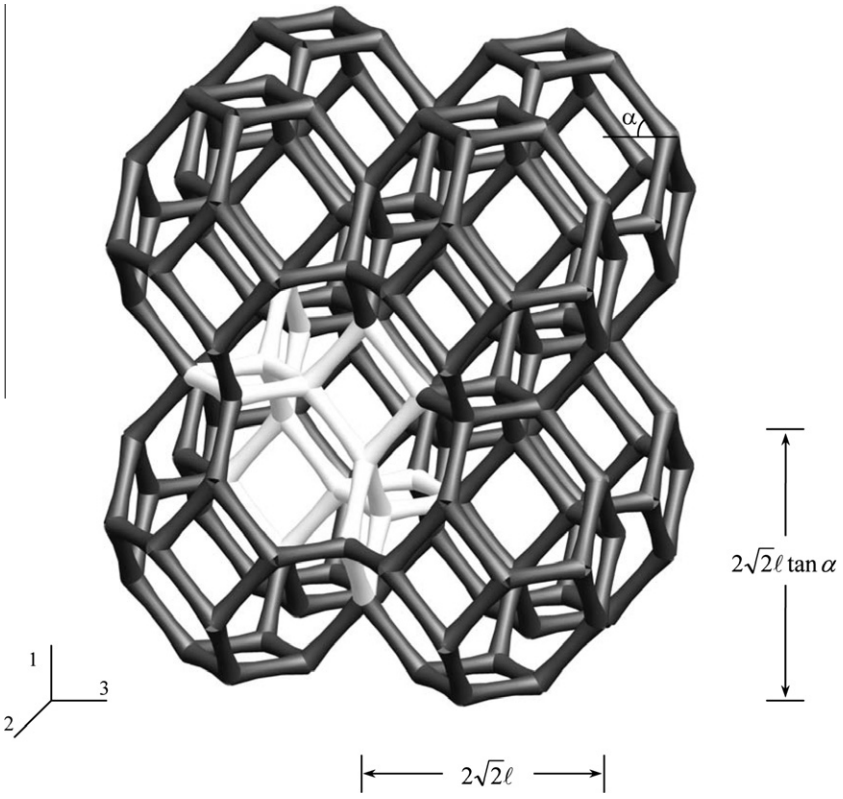

Fig. 7. Cluster of anisotropic Kelvin cells.

3.4. Discretization

The ligaments are discretized with finite elements within the nonlinear code ABAQUS using the B32, 3-node quadratic space beam element. Each ligament is represented by 8 elements of uniform cross sectional area that is based on $A = A_o f(\xi)$ as defined in the empirical fit of the measurements in Eq. (1). The values of $f(\xi)$ used are listed in Table 5. B32 elements are shear deformable as they include the strain energy due to transverse shear as follows (see ABAQUS manual for details):

$$U_s = \int_{-1/2}^{1/2} \beta \frac{V^2(\xi)}{2GA} \ell d\xi \quad \text{where } \beta = \frac{A}{I_y^2} \int_z \frac{Q^2(z)}{b(z)} dz \tag{6}$$

The second integral is over the cross section of the ligament (Fig. 5 in J & K-09II) with Q being the first moment of area about the y-axis and $b(z)$ the width; for circular cross sections $\beta = 10/9$ (V is the shear force and U_s the strain energy due to shear).

4. Results

We now use the three models outlined in Section 3 to predict the initial compressive response in the rise and transverse directions. The calculations will be terminated soon after the expected initial load maximum that represents the strength of the foam is reached. The material is elasto-plastic with the stress–strain response of the Al-6101-T6 alloy measured in a tensile test on a rod cast together with the foams tested (Ramberg–Osgood fit parameters $E = 10^4$ ksi (69 GPa), $\sigma_y = 28$ ksi (193 MPa), $n = 48$; see also Fig. 2 in J & K-09I).

4.1. Kelvin cell model

As has been shown in the past, because of the regularity of this idealized microstructure several of the mechanical properties of interest can be evaluated by considering just the characteristic cell (e.g., Dement'ev and Tarakanov, 1970a; Warren and Kraynik, 1997; Zhu et al., 1997; Laroussi et al., 2002; Gong and Kyriakides, 2005; Gong et al., 2005b; Mills, 2007; Jang et al., 2008). It is thus natural to start by compressing the fully periodic characteristic cell shown in Fig. 9 in which the ligaments have been assigned the geometric characteristics described in Section 3. Furthermore, in the first calculations a generic foam is considered with a relative density of $\rho^*/\rho = 0.08$ and an anisotropy of $\lambda = 1.2$ both of which approximately represent the average values of the three foams tested.

The cell is first compressed in the rise direction by prescribing incrementally the relative displacement ($\Delta\delta_1$) between the upper and lower periodic boundaries. The average stress σ_{11} required to produce this deformation is the force divided by the initial cross sectional area of the cell ($h_2 \times h_2$). Fig. 10(a) shows the calculated stress-displacement response. The stress is normalized by the initial elastic modulus of the foam, E_1^*, and the shortening, δ_1, by the height of the domain Nh_1 ($N = 1$ for this case). The initial part of the response is nearly linear with modulus E_1^* which is in very good agreement with measured values. The ligaments experience combined axial compression and bending that eventually cause the material to yield. Thus, in the neighborhood of point a inelastic action causes the response to become progressively softer. The progressive reduction in stiffness eventually results in a load maximum at point b (normalized stress and strain values $\{5.06 \times 10^{-3}, 0.0161\}$). Beyond this point (bc'), the single cell response has a negative slope indicating that localization may be possible in a larger domain.

The corresponding cell response for a linearly elastic material is drawn in the figure with a dashed line (oab'). It bifurcates into a long wave mode at a stress of $\sigma_{1Ce} = 0.163E_1^*$ and strain of 0.262, values that are much higher than those of the limit stress (see Fig. 7 in J & K-09-II).

By contrast, when the actual elasto-plastic stress–strain response of the Al alloy is used in the calculations no bifurcation is

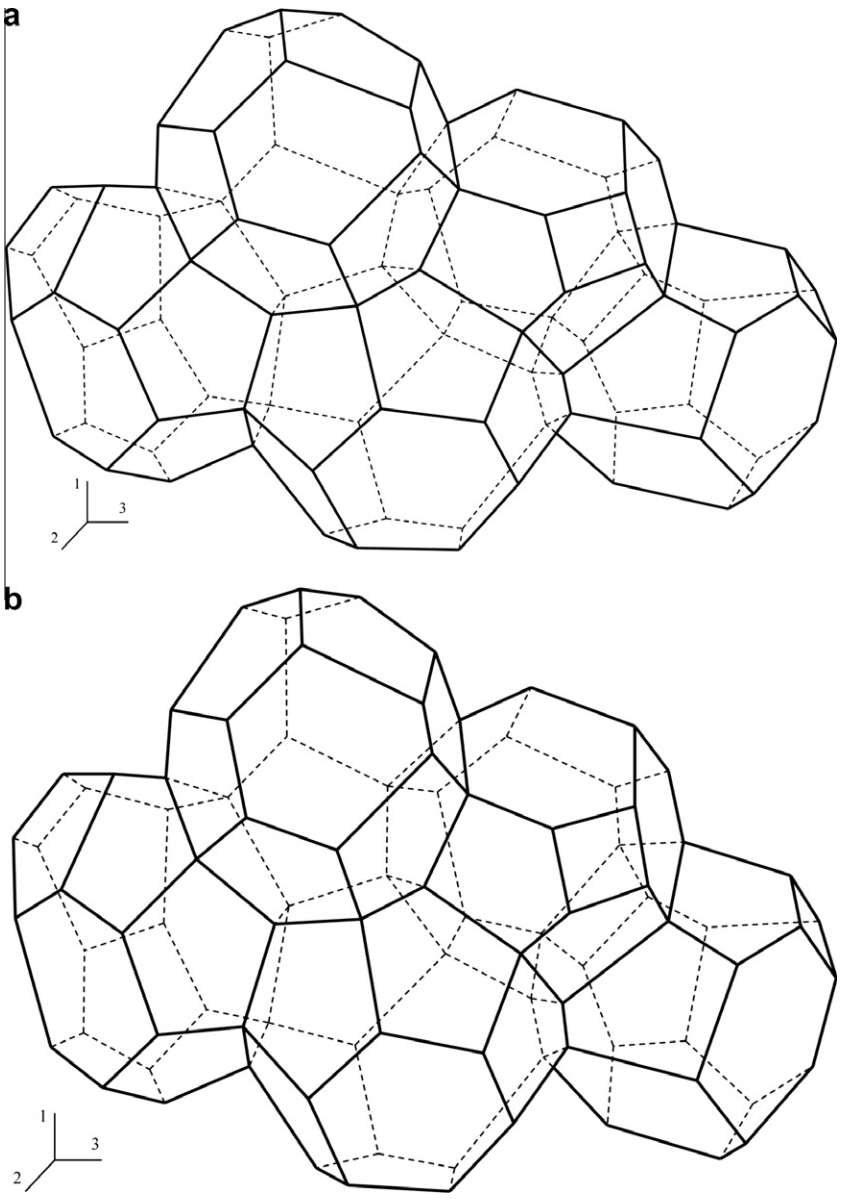

Fig. 8. (a) Skeletal drawing of a cluster of cells extracted from a random foam model. (b) The same cluster of cells after an anisotropy $\lambda = 1.30$ is applied.

Table 4
Fit parameters for correcting the relative density of Al foams with Eq. (5).

λ	n	k
1.00	1.7072	2.0263
1.10	1.7131	1.9543
1.20	1.7189	1.8985
1.30	1.7250	1.8561

Table 5
Cross-sectional area of beam elements in the foam ligaments.

ξ^a	$f(\xi)$
$0 \leqslant \lvert\xi\rvert \leqslant 0.2$	1
$0.2 < \lvert\xi\rvert \leqslant 0.3$	1.172
$0.3 < \lvert\xi\rvert \leqslant 0.4$	1.663
$0.4 < \lvert\xi\rvert \leqslant 0.5$	3.227

[a] $-1/2 \leqslant \xi(=x/\ell) \leqslant 1/2$.

detected between point a and the load maximum at b (the Bloch-wave method is used to check for possible bifurcations—Gong et al., 2005b). A limit load instability in the response of a characteristic cell implies that in a larger domain localized modes of deformation may be preferred. This possibility is investigated by considering a larger domain that is one characteristic cell thick and has 5×6 cells in the $x_1 - x_2$ plane. The domain has periodic boundaries at the top and bottom as well as the front and back but the two vertical sides are left free. The response of this domain, drawn in red[1] color in Fig. 10(a), coincides with that of the unit cell up to the local load maximum (point b). At higher displacements it traces a lower trajectory associated with localized shear buckling of two diagonal bands as shown in the deformed configuration in Fig. 10(b) (i) that corresponds to $\delta_1/5h_1 = 0.05$ (see similar results in Luxner et al. (2007)). Although always along the diagonals, the

[1] For interpretation of colour in figures, the reader is referred to the Web version of this article.

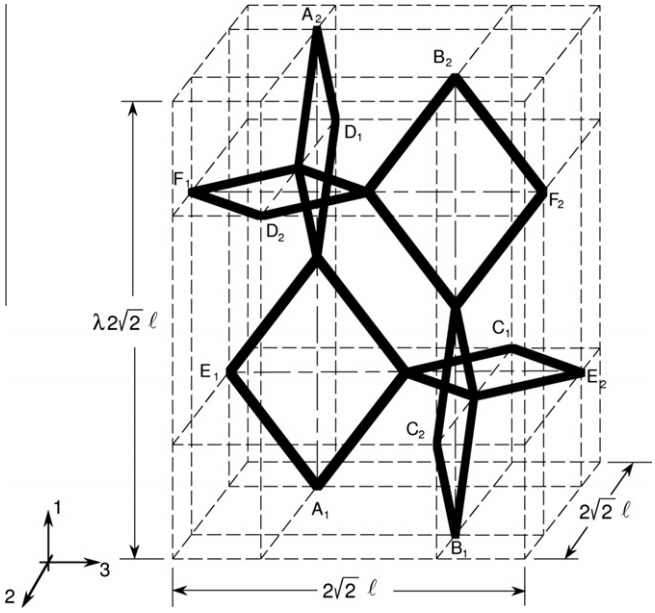

Fig. 9. The Kelvin foam characteristic cell.

localization patterns were shown in J & K-09II to depend on the domain size. Fig. 10(b) (ii) shows the deformed configuration at the same displacement ($\delta_1/6h_1 = 0.05$) for a 6×9 cells domain. Clearly the localization patterns are different from those of the smaller domain in image (i). This difference does not affect the response up to the limit load but was shown to affect to some degree the part of the crushing response that immediately follows it. The behavior observed has similarities to that of laterally loaded polymeric honeycombs reported in Papka and Kyriakides (1998). A difference is that in that problem the limit load was induced by a plastic bifurcation that led to localized collapse of horizontal rows of cells (see also Triantafyllidis and Schraad, 1998).

The unit cell was used to perform similar calculations for various foam densities in the range of interest keeping the anisotropy at $\lambda = 1.20$ which is close to the average of the values of the foams tested (see Table 1). Predictions of the strength (σ_{I1}) are included in Fig. 6(a) where they are seen to be in good agreement with the measured values.

Similar calculations were performed for compression in the transverse direction. Because of the anisotropy the material stiffness and strength are lower than those in the rise direction. However, the nature of the response is very similar and the strength can again be predicted using the unit cell. Numerical values of the transverse direction strength (σ_{I2}) are plotted in Fig. 6(b) where they are seen to be in good agreement with the experimental results. In summary, as reported in J & K-09II, the strengths of this Al foam can be evaluated with accuracy using the characteristic Kelvin cell. In such calculations the strength of the material appears as an initial load maximum in the compressive response.

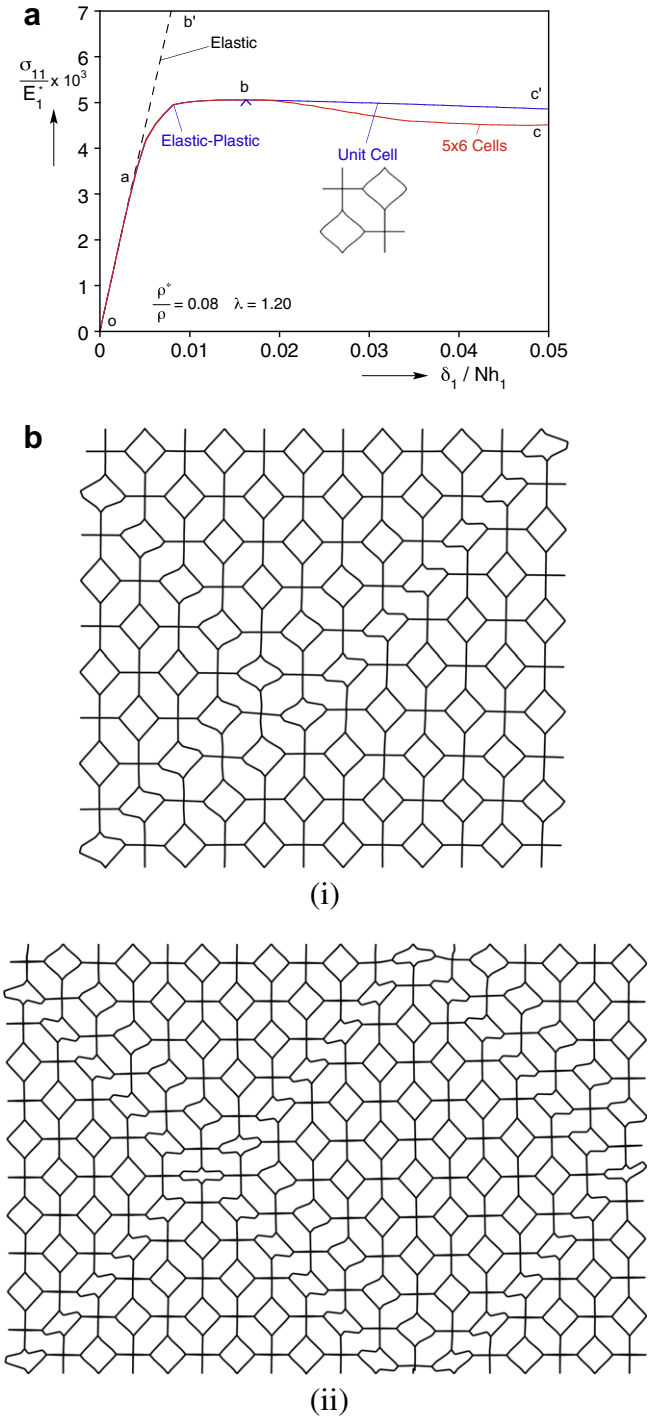

Fig. 10. (a) Calculated rise direction prebuckling and postbuckling stress-shortening responses. The prebuckling response comes from a single periodic cell and the postbuckling from a finite size domain. (b) Two deformed configurations corresponding to different domain sizes.

4.2. Perturbed Kelvin cell model

The perturbed Kelvin cell models that will be considered have three-dimensional domains with $\{6 \times 5 \times 6\}$ cells with periodic boundaries at the top and bottom but free lateral sides. Such a domain is first generated using regular Kelvin cells with the required anisotropy. The nodes of the cells are then perturbed randomly (amplitude ξ_o) in the manner described in Section 3. Three-dimensionality does not change the behavior in the early part of the response but, as we reported in J & K-09II, affects the onset of densification, which is beyond the scope of the current work. Calculations were performed for models with the generic values of relative density and anisotropy of $\rho^*/\rho = 0.08$ and $\lambda = 1.2$, and three values of the perturbation amplitude $\xi_o = 0.05, 0.10, 0.15$. The calculated rise direction stress-displacement responses are shown in Fig. 11(a) together with the one from the perfect microstructure. The responses are similar to those of the perfect structure. Interestingly, the limit stress is quite insensitive to this geometric imperfection but the trough that follows and the subsequent stress

undulation are influenced by ξ_o. Increasing ξ_o reduces the depth of the first trough as well as the amplitude of the undulations. (It is pointed out that because of the randomness of the applied perturbation, responses corresponding to the same ξ_o can differ slightly.) A possible explanation for this change can be seen in the comparison of the initial and two deformed configurations of the perfect case with ones from a case with $\xi_o = 0.15$ in Fig. 11(b). The perturbation of the nodes tends to break up the symmetry of the banded collapse localization of the perfect case. Instead, cell buckling and collapse are more randomly distributed and this tends to "smooth" the response.

Compression of perturbed domains in the transverse direction has similar effects on the calculated responses and consequently specific responses will not be presented. Perturbed Kelvin domains with $\xi_o = 0.15$ were used to evaluate the elastic moduli and strengths of foams in both directions. It should be noted that because of the randomness of the perturbation such results vary slightly from case to case. For this reason, the values that will be quoted represent averages of 10 sets of calculations. The predicted elastic moduli are slightly higher than the values predicted by the regular Kelvin model (see comparisons in Jang et al. (2008)). Predictions of the strengths in the two directions are included in Fig. 6(a) and (b). In both directions they are just slightly higher than the regular Kelvin model strengths.

4.3. Random foam model

The main random foam model that will be used has a cubical domain with $\{8 \times 8 \times 8\}$ cells. Anisotropy is introduced by elongating all cells in the x_1-direction in the manner described in Section 3.2. The ligaments are then "dressed" with solid beams in the manner described in Section 3.4. For chosen values of density and anisotropy and the average length of all ligaments in the model, the cross sectional area A_o at mid-span of each ligament is calculated from Eq. (5). Subsequently the length dependence of A_o is introduced using Eq. (2) and the scheme described in the last paragraph of Section 3.3. Guided by the behavior observed in the Kelvin cell model in calculations of the response including the anticipated load maximum, the two surfaces of the block that are compressed are made to be periodic while the four sides are left free.

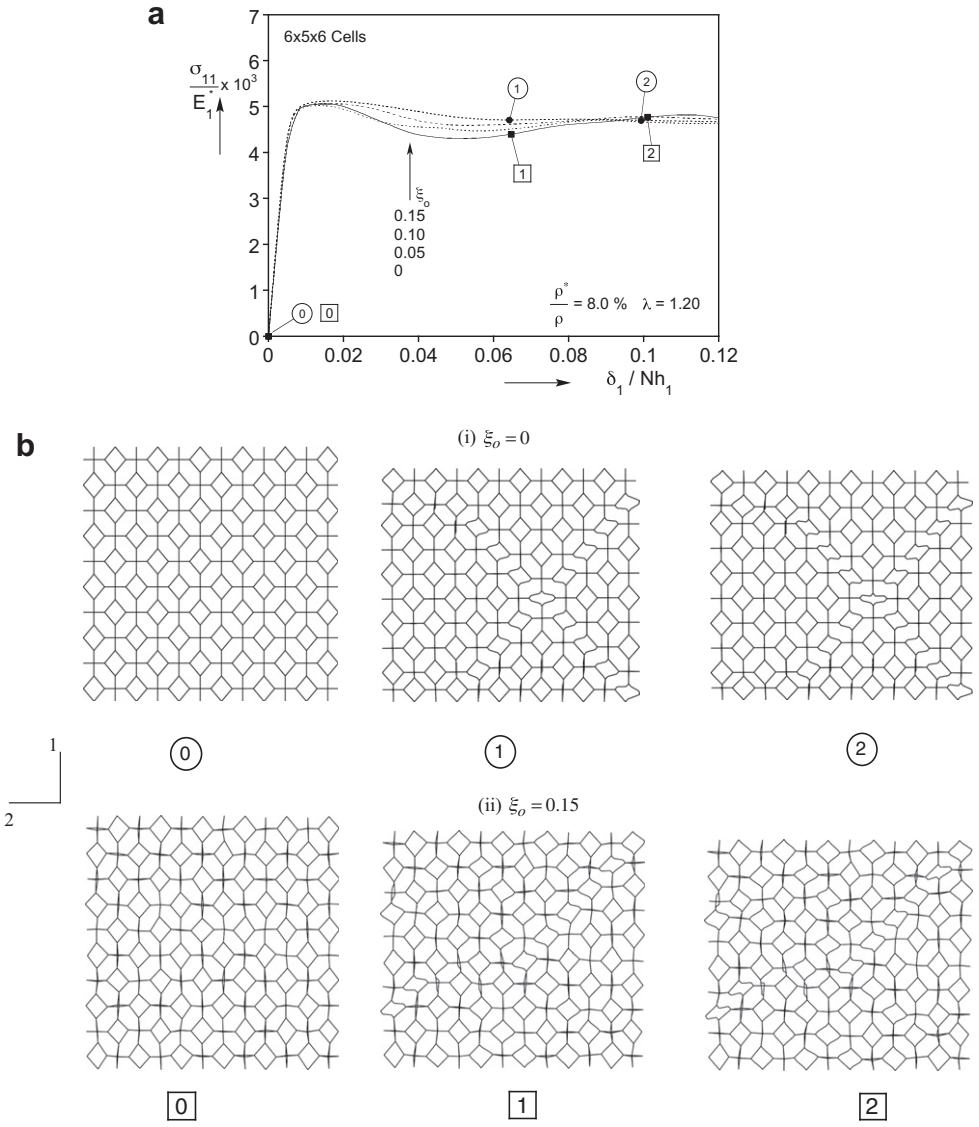

Fig. 11. (a) Initial stress–displacement responses for domains with different amounts of node perturbation. (b) Comparison of three deformed configurations for a perfect domain and one with $\xi_o = 0.15$.

The model is first evaluated by direct comparison to the response from Exp. R40–4 in which the foam had a relative density of 0.082 and an anisotropy of 1.18. Fig. 12(a) shows a comparison of the measured stress–displacement response and the one calculated up to a value of $\delta_1/H_1 = 10\%$ (H_1 is the height of the domain). The predicted response follows the experimental one quite closely. It exhibits a limit load at a stress and strain of {423 psi, 1.64%}, which compare with {406 psi, 1.65%} from the experiment. The two responses also agree quite well beyond the limit load although at values of average strain corresponding to the local minimum and beyond the numerical results are no longer dependable as contact of ligaments in the collapsing cells commences which is not included in the random model calculations.

Fig. 12(b) shows two deformed configurations of the skeletal version of the compressed model. The deformation measure found to best represent the localization that develops is the magnitude of the "rotation" of the beam ligaments. The rotation is calculated in each node of the beams while between two nodes the values are interpolated. The code stores the three components of a rotation vector $\boldsymbol{\phi}$ for all nodes. The vector $\boldsymbol{\phi}$ is defined by amplitude $\phi = \|\boldsymbol{\phi}\|$ and a rotation axis $\boldsymbol{P} = \boldsymbol{\phi}/\|\boldsymbol{\phi}\|$. The rotation vector $\boldsymbol{\phi}$ then consists of a rotation ϕ (radians) around the axis $\boldsymbol{P}$. Drawn in color in the deformed configurations is the magnitude of ϕ. Configuration ① is a frontal view of the foam block analyzed at $\delta_1/H_1 = 4.58\%$. The rotation distribution indicates that localized deformation along inclined directions has developed. The localization is more pronounced in configuration ② that corresponds to $\delta_1/H_1 = 9.03\%$ (shown for illustrative purposes only as some ligament contact would have commenced by this point). The localization is seen to form along inclined directions but the patterns are disorganized and vary through the depth of the block. The patterns seen differ significantly from those in the Kelvin cell domain in Fig. 11(b); indeed they much more resemble crushing patterns seen in the experiments reported in J & K-09I.

Since the vertical sides of the domain analyzed are free, the sensitivity of such responses to the domain size must be considered. To this end cubical random microstructure domains of different sizes were generated in approximately the same manner. The skeletal domains were first elongated in the x_1-direction to an anisotropy of $\lambda = 1.2$ and made into foams with relative density of 8.0% by dressing them with appropriate beams as described earlier. The models were then compressed in the same manner as the case described above. It must be pointed out that no two such random microstructures are the same. Consequently, the responses of any two such models of the same size are never the same. For this reason several models of the same size were considered in order to establish the trend. Fig. 13 shows a comparison of the compressive responses from three representative models with $\{10 \times 10 \times 10\}$, $\{8 \times 8 \times 8\}$ and $\{6 \times 6 \times 6\}$ cells. The results show that there is a stiffening effect as the domain size increases primarily because the role of the free edges becomes less important as the domain volume increases. For the results shown, the elastic modulus E_1^* for the 10^3 model is 3.1% higher than the 8^3 model while the value for the 6^3 model is 7.4% lower. The stress maximum, σ_{I1}, increases with size also, so for the larger domain it is 5.6% higher than the 8^3 model and for the smaller one it is 5.1% smaller. As pointed out these results can be viewed as averages of several runs for each domain size.

8^3 cell models are now used to conduct a limited parametric study of random foams. In an effort to best represent an infinite foam medium, when calculating the elastic moduli the cubical domain is made to be fully periodic (as was done in Jang et al. (2008)). Thus, for example for $\rho^*/\rho = 8.0\%$ this scheme yields E_1^* and E_2^* values that are respectively 10.9% and 12% higher than the corresponding finite size domains. This difference tends to decrease as the domain size considered increases. Predictions for the rise- and transverse direction moduli for various relative density values

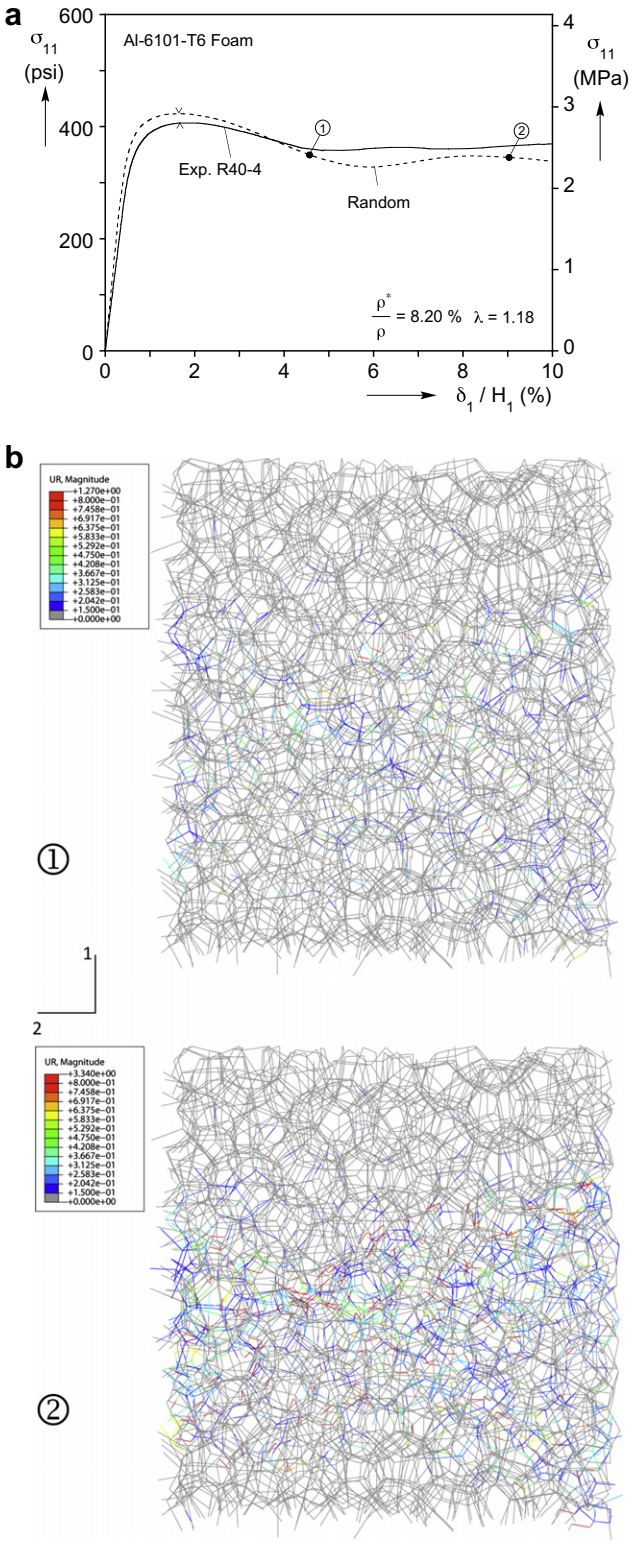

Fig. 12. (a) Comparison of random foam model and experimental stress–displacement responses in rise direction. (b) Frontal views of deformed configurations corresponding to points ① and ② on the calculated response shown in Fig. 12a.

in the range of interest are included in Fig. 29 of Jang et al. (2008). They are somewhat higher than the predictions from the Kelvin cell model for both directions but lie within the scatter of the experimental results.

Calculations of the initiation stresses were performed using the same 8^3 cell models with the four lateral sides were left free.

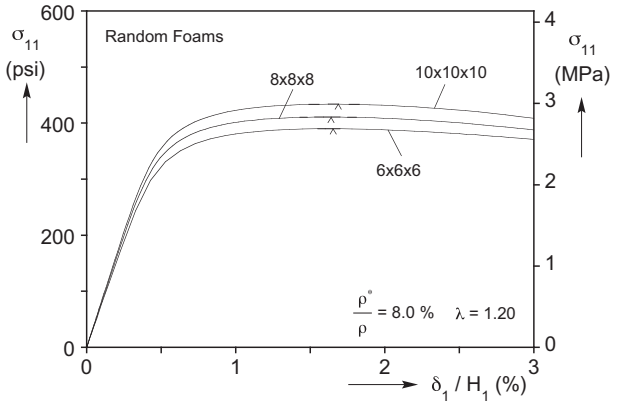

Fig. 13. Comparison of calculated stress–displacement responses from random foam models of different size domains.

Results for the two foam directions as a function of relative density are included in Fig. 6(a) and (b). The random foam models yield slightly higher values of σ_I than the two Kelvin cell models for both directions but the predictions remain close to the measurements.

5. Summary and conclusions

The microstructure of Al open-cell foams was previously characterized using micro-computed X-ray tomography. The characterization includes measurement of cell size and anisotropy, ligament length distribution and distribution of cross sectional area along the length of the ligaments. Foams of three cell sizes were considered: 10, 20 and 40 ppi, with anisotropies in the range of 1.18–1.27. The foam ligaments had rounded, convex cross sections and a nearly symmetric distribution of material along the length with the mid-span being the slimmest.

The measured geometric characteristics were used to build two families of FE foam models. In the first family, the foams were idealized as regular Kelvin cells loaded in the <100> and <010> directions. A derivative of the Kelvin cell model consists of $N \times N \times N$ Kelvin cells whose nodes have been randomly perturbed. The second family of models consists of realistic random foam domains that contain N^3 cells generated with the Surface Evolver software. In all models the cells are elongated in the <100> direction; the ligaments are assumed to be straight and to have circular cross sections with variable areas along the length. The ligaments were discretized as shear deformable beams.

In all calculations the compressive response starts with a linearly elastic regime. At higher stress levels plastic action causes a gradual reduction of the stiffness, which eventually leads to a stress maximum that represents the strength of the material. The periodicity of the Kelvin cell enables calculation of the compressive response up to the limit stress with just a single fully periodic characteristic cell. Beyond the limit stress, deformation localizes along the principal diagonals of the microstructure and for this reason it was evaluated using finite size 3-D domains that allow the localization to develop. The perturbed Kelvin models involved 8^3 cell domains with periodic compressed ends but free on the sides. The compressive response is also characterized by a limit load instability but the localized buckling patterns are now less organized. The elastic modulus and the limit stress were not sensitive to the domain size while the subsequent response was to some degree. The random models had 6^3, 8^3 or 10^3 cells with similar boundary conditions to the perturbed Kelvin models. The compressive response is similar to that of the Kelvin models but now the localization is totally disorganized resembling that observed in experiments. In this case, both the elastic modulus and strength increased somewhat as the domain became larger. For this reason the elastic properties reported were calculated with fully periodic boundaries.

The performance of the models was then compared to measured values of the elastic moduli and strengths in the rise and transverse directions. The following observations can be made from this comparison.

- Predictions of the elastic moduli from the three models reported in Jang et al. (2008) compared well with measurements for both directions.
- The three models yielded foam strengths that were close to each other and also compared favorably to the experimental results. This was the case despite the clearly different localization patterns that develop after the limit stress in each model.

Thus, despite some differences in the post-limit load response and the associated localization patterns produced by the three types of models, they yield comparable elastic properties and compressive strengths. In other words, a single periodic Kelvin cell and a much larger domain occupied by a random foam yield comparable results. This indicates that inelastic ligament bending is a major player in the compressive response. Consequently, accurate representation of the ligament bending rigidity and the base material response are essential. By contrast, the randomness of the actual microstructure in nearly monodisperse foams appears to play a secondary role. Clearly, the simplicity of the Kelvin cell model makes it an attractive engineering tool for estimating these foam properties.

Acknowledgments

The authors acknowledge with thanks the financial support of the work by the National Science Foundation through Grant CMS-0856155. The authors also wish to thank B.D. Leyda and ERG for providing the Duocel aluminum foam samples used in the study to our specifications.

Appendix A. Numerical generation of random foams

Random spatially periodic soap froth is generated using Brakke's Surface Evolver (1992) (Kraynik et al., 2003). A primitive Voronoi froth with foam-like characteristics is first generated from randomly packed monodisperse hard spheres using molecular dynamics. Each Voronoi cell consists of all points that lie closest to a random seed, i.e., the center of each sphere. The Voronoi structure is then used as an initial condition in the Surface Evolver to generate a "dry" foam in which the liquid volume fraction is zero and the films can be modeled as two-dimensional surfaces. The software minimizes energy and balances mechanical forces by satisfying Plateau's laws: I. *the faces of cells are surfaces of constant mean curvature; II. three faces meet at equal dihedral angles of 120°*; and III. *four edges meet at the tetrahedral angle* $\cos^{-1}(-1/3) \approx 109.47°$. For monodisperse foam the additional constraint that all cells have the same volume is also applied. The relaxation process requires a large number of topological transitions that involve cell-neighbor switching. Since the solution is a local energy minimum, the surface area can be further reduced by subjecting the foam to large-deformation tension–compression cycles that provoke additional neighbor switching (*annealing*). The resulting structures are in very good agreement with Matzke's experimental study (1946) of monodisperse soap froth regarding types of polyhedra, distribution of polygonal sides, and ligament length distribution (see Kraynik, 2003; Kraynik et al., 2003, 2004, 2005, 2006). The skeletal

versions of such random microstructures used in this study are formed by joining the cell vertices with straight lines.

References

ABAQUS Manual 6.8.

Ashby, M.F., Evans, A., Fleck, N.A., Gibson, L.J., Hutchinson, J.W., Wadley, H.N.G., 2000. Metal Foams: A Design Guide. Butterworth-Heinemann.

Brakke, K.A., 1992. The Surface Evolver. Exp. Math. 1, 141–165 <http://www.susqu.edu/facstaff/b/brakke/evolver/>.

Dement'ev, A.G., Tarakanov, O.G. 1970a. Effect of cellular structure on the mechanical properties of plastic foams. Mekhanika Polimerov No. 4, 594-602-865. Translation pp. 519–525.

Dement'ev, A.G., Tarakanov, O.G. 1970b. Model analysis of the cellular structure of plastic foams of the polyurethane type. Mekhanika Polimerov No. 5, 859-865. Translation pp.744–749.

Gibson, L.J., Ashby, M.F., 1997. Cellular Solids: Structure and Properties, second ed. Cambridge University Press.

Gong, L., Kyriakides, S., 2005. Compressive response of open-cell foams. Part II: initiation and evolution of crushing. Int. J. Solids Struct. 42, 1381–1399.

Gong, L., Kyriakides, S., 2006. On the crushing stress of open cell foams. ASME J. Appl. Mech. 73 (5), 807–814.

Gong, L., Jang, W.-Y., Kyriakides, S., 2005a. Compressive response of open-cell foams. Part I: morphology and elastic properties. Int. J. Solids Struct. 42, 1355–1379.

Gong, L., Kyriakides, S., Triantafyllidis, N., 2005b. On the stability of Kelvin cell foams under compressive Loads. J. Mech. Phys. Solids 53 (4), 771–794.

Hilyard, N.C., Cunningham, A. (Eds.), 1994. Low Density Cellular Plastics: Physical Basis of Behavior. Chapman & Hall, London.

Jang, W.-Y., Kyriakides, S., 2009I. On the crushing of aluminum open-cell foams: part I experiments. Int. J. Solids Struct. 46, 617–634.

Jang, W.-Y., Kyriakides, S., 2009II. On the crushing of aluminum open-cell foams: part II analysis. Int. J. Solids Struct. 46, 635–650.

Jang, W.-Y., Kraynik, A.M., Kyriakides, S., 2008. On the microstructure of open-cell foams and its effect on elastic properties. Int. J. Solids Struct. 45, 1845–1875.

Kraynik, A.M., 2003. Foam structure: From soap froth to solid foams. MRS Bull. 28 (4), 275–278.

Kraynik, A.M., 2006. The structure of random foam. Adv. Eng. Mater. 8 (9), 900–906.

Kraynik, A.M., Reinelt, D.A., van Swol, F., 2003. Structure of random monodisperse foam. Phys. Rev. E 67, 0314031/1–0314031/4.

Kraynik, A.M., Reinelt, D.A., van Swol, F., 2004. Structure of random foam. Phys. Rev. Lett. 93 (20), 208301/1–208301/4.

Kraynik, A.M., Reinelt, D.A., van Swol, F., 2005. Structure of random bidisperse foam. Colloids Surf. A 263, 11–17.

Laroussi, M., Sab, K., Alaoui, A., 2002. Foam mechanics: nonlinear response of an elastic 3D-periodic microstructure. Int. J. Solids Struct. 39, 3599–3623.

Luxner, M.H., Stampfl, J., Pettermann, H.E., 2007. Numerical simulations of 3D open cell structures-influence of structural irregularities on elasto-plasticity and deformation localization. Int. J. Solids Struct. 44, 2990–3003.

Matzke, E.B., 1946. The three-dimensional shape of bubbles in foam – An analysis of the role of surface forces in three-dimensional shape determination. Am. J. Bot. 33, 58–80.

Mills, N.J., 2007. The high strain mechanical response of the wet Kelvin model for open-cell foams. Int. J. Solids Struct. 44, 51–65.

Papka, S.D., Kyriakides, S., 1998. In-plane crushing of a polycarbonate honeycomb. Int. J. Solids Struct. 35, 239–267.

Thompson, W.(Lord Kelvin), 1887. On the division of space with minimal partitional area. Philos. Mag. 24 (5th Series), 503–514.

Triantafyllidis, N., Schraad, M., 1998. Onset of failure in aluminum honeycombs under general in-plane loading. J. Mech. Phys. Solids 46, 1089–1124.

Warren, W.E., Kraynik, A.M., 1997. Linear elastic behavior of a low-density Kelvin foam with open cells. ASME J. Appl. Mech. 64, 787–793.

Weaire, D., Hutzler, S., 1999. The Physics of Foams. Oxford University Press, Oxford.

Zhou, J., Mercer, C., Soboyejo, W.O., 2002. An investigation of the microstructure and strength of open-cell 6101 aluminum foams. Metall. Mater. Trans. 33A, 1413–1427.

Zhou, J., Shrotriya, P., Soboyejo, W.O., 2004. Mechanisms and mechanics of compressive deformation in open-cell Al foams. Mech. Mater. 36, 781–797.

Zhu, H.X., Knott, J.F., Mills, N.J., 1997. Analysis of the elastic properties of open-cell foams with tetrakaidecahedral cells. J. Mech. Phys. Solids 45, 319–343.